Electrochemistry Communications 88 (2018) 83–87

Contents lists available at ScienceDirect

Electrochemistry Communications

journal homepage: www.elsevier.com/locate/elecom

Step-by-step synthesis of a heteroatom-doped carbon-based electrocatalyst for the oxygen reduction reaction

Tatiana A. Lastovina[a,*], Andriy P. Budnyk[a], Yulia A. Pimonova[a], Aram L. Bugaev[a], Alexey G. Fedorenko[c], Vladimir P. Dmitriev[a,b]

[a] International Research Center "Smart Materials", Southern Federal University, 344090 Rostov-on-Don, Russia
[b] SNBL at European Synchrotron Radiation Facility, 38000 Grenoble, France
[c] Modern Microscopy Center, Academy of Biology and Biotechnology, Southern Federal University, 344090 Rostov-on-Don, Russia

ARTICLE INFO

Keywords:
Co
Zn-ZIF
Carbon-based electrocatalyst
Oxygen reduction reaction
Fuel cells

ABSTRACT

A heteroatom-doped carbon-based electrocatalyst for the oxygen reduction reaction (ORR) was prepared from a hybrid zeolitic imidazolate framework (ZIF) using a step-by-step approach. A bimetallic Co,Zn-ZIF was synthesized by a microwave-assisted method and then enriched with Fe and N. The resulting ZIF was pyrolysed at 700 °C in an inert atmosphere, producing a complex morphology including an amorphous carbon matrix, cobalt nanoparticles and bamboo-like nanotubes. A range of techniques were used to characterize the initial ZIF and the resulting catalyst. The catalytic activity and stability of the carbon-based electrocatalyst towards the ORR were investigated by cyclic voltammetry and chronoamperometry using a rotating disc electrode (RDE) in an acidic medium. The highest electrocatalytic activity for the ORR was reached when an equal weight of commercial carbon black (Vulcan XC-72) was added to the composite. Analysis of Koutecky–Levich plots showed that the reaction followed a four-electron transfer mechanism. A durability test over 1000 cycles showed no signs of decreasing catalytic activity. This catalyst appears to be a promising material for application in fuel cells.

1. Introduction

Advances in clean energy technologies depend on the development of cheap and efficient materials for energy storage and conversion. The growing number of fuel-cell-powered electric vehicles is stimulating improvements in fuel cells aimed at reducing their cost and increasing their lifetime [1]. The function of an air–hydrogen fuel cell is limited by the oxygen reduction reaction (ORR), which relies on the presence of a catalyst [2]. The most efficient platinum-based catalysts are not suitable for large-scale commercial application, primarily due to their high cost, poor durability and limited natural reserves. The development of new ORR electrocatalysts is proceeding along two main pathways: (i) lowering the Pt content by forming core-shell or skeleton structures, Pt–transition metal alloys, etc. [3], or (ii) replacing Pt with other materials [4]. In the latter case, heteroatom-doped carbon materials (HDCM) produced by the pyrolysis of metal-organic frameworks (MOFs) are likely to achieve the desirable activity and stability towards ORR [5–8].

Efficient Pt-free HDCMs are frequently prepared from zeolitic imidazolate frameworks (ZIFs), resulting in a uniform distribution of heterogeneous atoms in a carbon matrix [9]. The Pt-free HDCMs can be further modified using metal ions and nitrogen atoms to form metal/nitrogen/carbon (M/N/C, M = Fe or Co) catalysts for the ORR, which are stable in alkaline or acid solutions [10,11]. It has also been reported that (Fe,Zn)/N/C and (Fe,Co)/N/C systems have been obtained from monometallic MOFs after doping with iron cations [9,12]. Wang et al. [13] reported the preparation of MOF-253 materials enriched with Fe and N using $FeCl_2$ and 1,10-phenanthroline in acetonitrile. The resulting porous carbon-based materials demonstrated excellent ORR activity.

To the best of our knowledge, a HDCM containing all the metals mentioned above (Zn,Co,Fe) in a nitrogen-rich, carbon-based material has not been studied with respect to catalysis of the ORR. In this work, we prepared a Co,Zn-ZIF material using a microwave-assisted synthesis. The product was enriched with Fe and N-containing species and then pyrolysed to produce the HDCM. An ORR test in an acidic medium confirmed its durability. We also found that addition of an equal weight of commercial carbon black (Vulcan XC-72) to the sample increased its catalytic activity.

2. Experimental

2.1. Preparation of the catalyst

N,N-dimethylformamide (DMF) solution containing Co$(NO_3)_2{\cdot}6H_2O$, Zn$(NO_3)_2{\cdot}6H_2O$ and 2-methylimidazole (mIm) in a molar

* Corresponding author.
E-mail address: lastovina@sfedu.ru (T.A. Lastovina).

https://doi.org/10.1016/j.elecom.2018.02.002
Received 6 December 2017; Received in revised form 1 February 2018; Accepted 1 February 2018
Available online 05 February 2018
1388-2481/

ratio of 2:1:6 was heated using a microwave system MARS 6 (CEM) at 140 °C for 120 min under stirring. The resulting powder was collected by centrifugation, washed with DMF and methanol, kept in methanol for 24 h, and dried at 80 °C. The powder was then impregnated with 1,10-phenanthroline and $Fe(CH_3COO)_2$ in a molar ratio of 330:100:16 in ethanol. After sonication for 30 min and stirring for 1 h, the powder was dried at 80 °C. Finally, the powder was calcined at 700 °C for 3 h under an argon flow in a tube furnace (Nabertherm) at a heating rate of 10 °C min^{-1}.

2.2. Characterization of the catalyst

X-ray diffraction patterns (XRD) were collected at the BM01 beamline of the European Synchrotron Radiation Facility (ESRF, Grenoble, France) using λ = 0.7225 Å radiation. High energy resolution fluorescence detection (HERFD) and X-ray adsorption near-edge structure (XANES) spectra were measured at the ID26 beamline of the ESRF. In addition, we used a M4 TORNADO (Bruker) Micro X-ray fluorescence (XRF) spectrometer, a Raman analyzer 100 (Renishaw), a G2 Spirit BioTWIN (Tecnai) transmission electron microscope (TEM), a Zeiss Supra 25 scanning electron microscope (SEM), a FTIR spectrometer Vertex 70 (Bruker), simultaneous thermal analyzer 449 F5 (Netzsch), and a surface area analyzer ASAP 2020 (Micromeritics) to characterize the structure of the prepared materials.

2.3. Electrochemical experiments

The electrochemical measurements were performed at room temperature in a typical three-electrode cell in 0.1 M $HClO_4$ solution with a Pt counter electrode and Ag/AgCl (sat. KCl solution) reference electrode. The electrochemical properties of the prepared HDCM were investigated by cyclic voltammetry (CV) and linear sweep voltammetry (LSV). The catalytic ink was prepared by mixing 3 mg of the HDCM sample with 3 mg of commercial carbon black (Vulcan XC-72). This was then dispersed in a solution containing 900 μl of isopropanol and 100 μl of 0.5% Nafion solution (DuPont). After sonication and stirring to form a uniform black ink, 28 μl of the catalyst ink was dripped onto a glassy carbon surface (0.19625 cm^2) and dried in air. To find the composition of ink with the highest catalytic activity, inks containing the fabricated HDCM (denoted '0 wt%'), pure Vulcan ('100 wt%'), as well as mixtures of HDCM and Vulcan in weight ratios of 1:1 and 1:2 ('50 wt%' and '67 wt%', respectively), were separately prepared and tested. The total loading of carbon materials was 412 μg·cm^2.

The CV curves were measured at 1600 rpm with a scan rate of 20 mV·s^{-1}. After each 100 cycles, LSV curves were recorded at different speeds with a scan rate of 5 mV·s^{-1}.

Chronoamperometric measurements were carried out at a static cathodic potential (0.6 V vs. RHE) with an electrode rotation rate of 1600 rpm in oxygen-saturated 0.1 M $HClO_4$ solution.

3. Results and discussion

According to the XRF data, the as-synthesized Co,Zn-ZIF contained 29.3 wt% of Co and 70.7 wt% of Zn, which corresponds to a molar ratio of Co:Zn = 1:2.2 ($CoZn_{2.2}$-ZIF). After impregnation, this material was denoted $CoZn_{2.2}$-ZIF-Fe-phen. The pyrolysed carbonaceous material ($FeCo_{14}Zn_{23}$/N/C) was found to contain Co and Zn in the molar ratio 1:1.64. The Fe content was 2.32 wt% to both cobalt and zinc, so the molar ratio of Fe:Co:Zn was 1:14.26:23.33. After pyrolysis, a reduction (~25%) of Zn content was observed in the final material. Such Zn depletion has been previously observed in a similar system [14].

The XRD pattern of the $CoZn_{2.2}$-ZIF is depicted in Fig. 1a. This material shows the ZIF-8 sodalite topology [15]. In contrast, the $FeCo_{14}Zn_{23}$/N/C exhibited very low crystallinity. Resolution of the very weak XRD peaks from the diffuse scattering background was possible only by utilizing a high-quality synchrotron-based XRD signal. The most intense diffraction peaks are characteristic of fcc cobalt, suggesting the

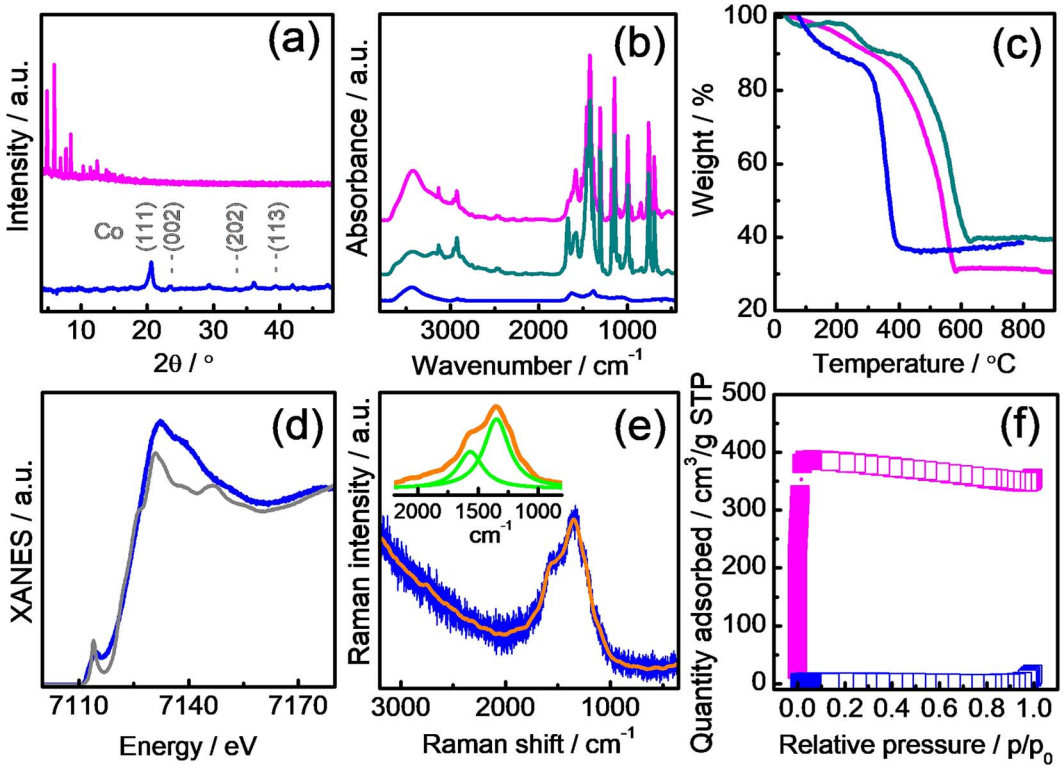

Fig. 1. Characterization results for $CoZn_{2.2}$-ZIF (magenta), $CoZn_{2.2}$-ZIF-Fe-phen (cyan) and $FeCo_{14}Zn_{23}$/N/C (blue) samples: (a) XRD patterns; (b) FTIR spectra; (c) TGA curves measured in N_2 (magenta, cyan) and in air (blue); (d) HERFD-XANES spectrum including Fe_3O_4 as reference (grey); (e) Smoothed Raman spectrum (orange). The inset shows the main contributors (green) to the band; (f) N_2 sorption isotherms. (For interpretation of the references to color in this figure legend, the reader is referred to the web version of this article.)

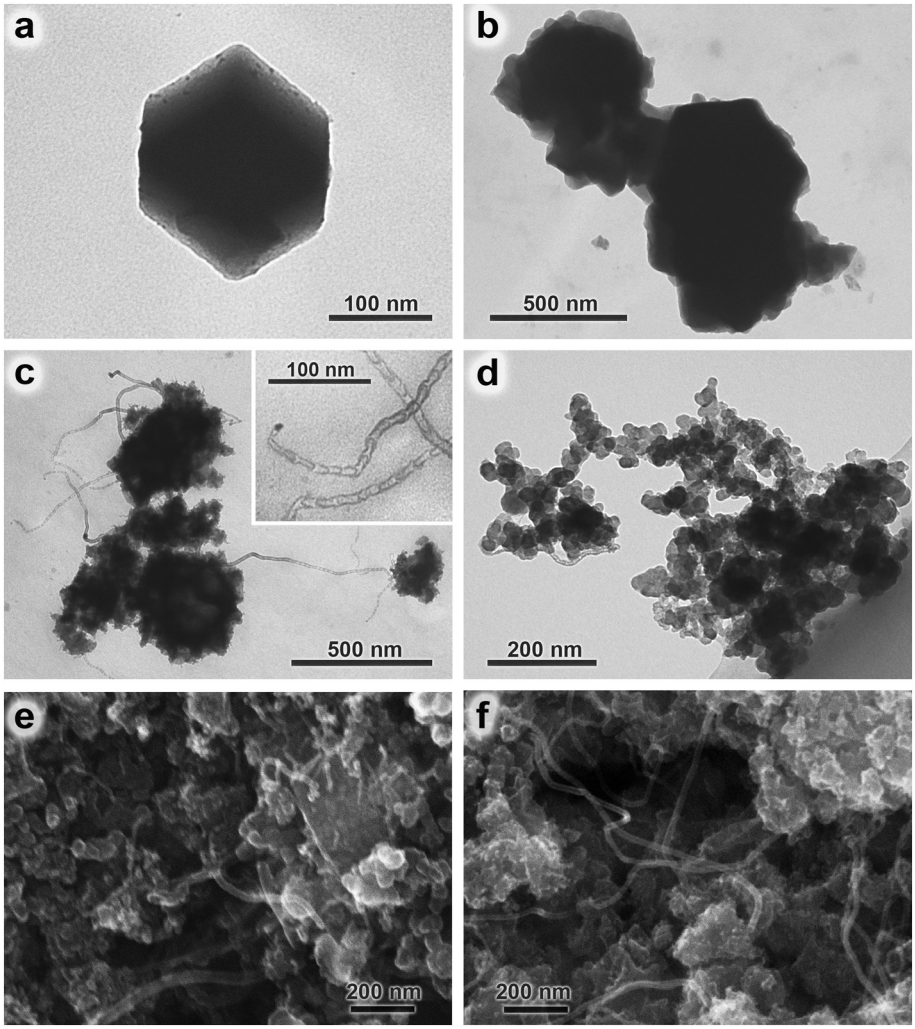

Fig. 2. (a–d) TEM images of (a) $CoZn_{2.2}$-ZIF and (b) $CoZn_{2.2}$-ZIF-Fe-phen starting MOFs, the $FeCo_{14}Zn_{23}$/N/C composite after (c) carbonisation at 700 °C and after (d) 1000 CV cycles of ORR testing; (e–f) SEM micrographs of the $FeCo_{14}Zn_{23}$/N/C composite before (e) and after (f) 1000 cycles. The inset in (c) shows an enlarged image of the $FeCo_{14}Zn_{23}$/N/C.

formation of Co NPs. The size of the nanoparticles was about 5.6 nm (estimated using the Scherrer equation).

The FTIR spectra of $CoZn_{2.2}$-ZIF and $CoZn_{2.2}$-ZIF-Fe-phen in Fig. 1b show the vibrational profile of the imidazolate linker in ZIF-8 [15]. The two bands at 1670 and 1579 cm^{-1} can be attributed to the carboxylate group in the acetate anion in $CoZn_{2.2}$-ZIF-Fe-phen. After calcination at 700 °C, the spectral profile changed dramatically, eroding into an almost featureless line with weak bands due to physisorbed water and some carbonaceous residuals.

The TGA curves for both $CoZn_{2.2}$-ZIF and $CoZn_{2.2}$-ZIF-Fe-phen samples (Fig. 1c) were measured in an inert atmosphere to determine the weight loss occurring during the pyrolysis, while that of Fe-$Co_{14}Zn_{23}$/N/C was performed in air. The curves show three distinct stages: a moderate decline of ~10% at temperatures up to 300 °C due to the removal of physisorbed water and entrapped solvent molecules; a rapid fall (50–60%) in the range 400–600 °C attributed to the collapse of the structure [15]; finally, thermal stability at temperatures higher than 600 °C. The $CoZn_{2.2}$-ZIF-Fe-phen sample differed in having an extra step at ~250 °C, higher thermal stability (+50 °C) and a smaller total weight loss (10% less).

We probed the state of iron in $FeCo_{14}Zn_{23}$/N/C using Fe *K*-edge HERFD-XANES spectroscopy. The profile of the XANES spectrum in Fig. 1d indicates that iron was present and that its oxidation state was close to that of iron in Fe_3O_4. However, there was no direct evidence of any iron oxide phase from XRD (Fig. 1a) or FTIR (Fig. 1b).

The Raman spectrum of $FeCo_{14}Zn_{23}$/N/C collected with a 785 nm laser is depicted in Fig. 1e. A complex band at ~1360 cm^{-1} was observed, which is typical of amorphous carbon [16]. The smoothed and baseline-corrected spectrum was fitted using Lorentzians. The two main components at 1564 and 1346 cm^{-1} (inset in Fig. 1e) corresponds to characteristic G- and D-bands [17]. The intensity ratio, I_D/I_G, was 1.88, suggesting a low degree of graphitisation in this N-doped carbon.

The nitrogen sorption isotherm for $CoZn_{2.2}$-ZIF (Fig. 1f) was of type I (IUPAC), which is typical of microporous materials. The BET specific surface area for $CoZn_{2.2}$-ZIF was 1402 m^2/g with a corresponding Langmuir value of 1685 m^2/g. The uptake of $FeCo_{14}Zn_{23}$/N/C is very low, with BET and Langmuir values of 19 and 23 m^2/g, respectively.

The $CoZn_{2.2}$-ZIF consists of rhombic dodecahedron crystals, as can be seen in Fig. 2a. After impregnation, the MOF crystals appear to be sticking together (Fig. 2b). The pyrolysed material (Fig. 2c) comprises an amorphous matrix doped with NPs and bamboo-shaped carbon nanotubes (CNTs). After 1000 cycles in the ORR test the catalyst had better separated NPs (Fig. 2d) compared with the pure catalyst (Fig. 2c).

The most distinct feature of the composite's morphology is the bamboo-like strings protruding from the agglomerates. These are the CNTs, which are known to be formed with the aid of cobalt nanoparticles, situated in the head of the developing tube (see enlarged inset in Fig. 2c). Such structures have already been observed in similar systems, and a growth mechanism for these bamboo-like structures has

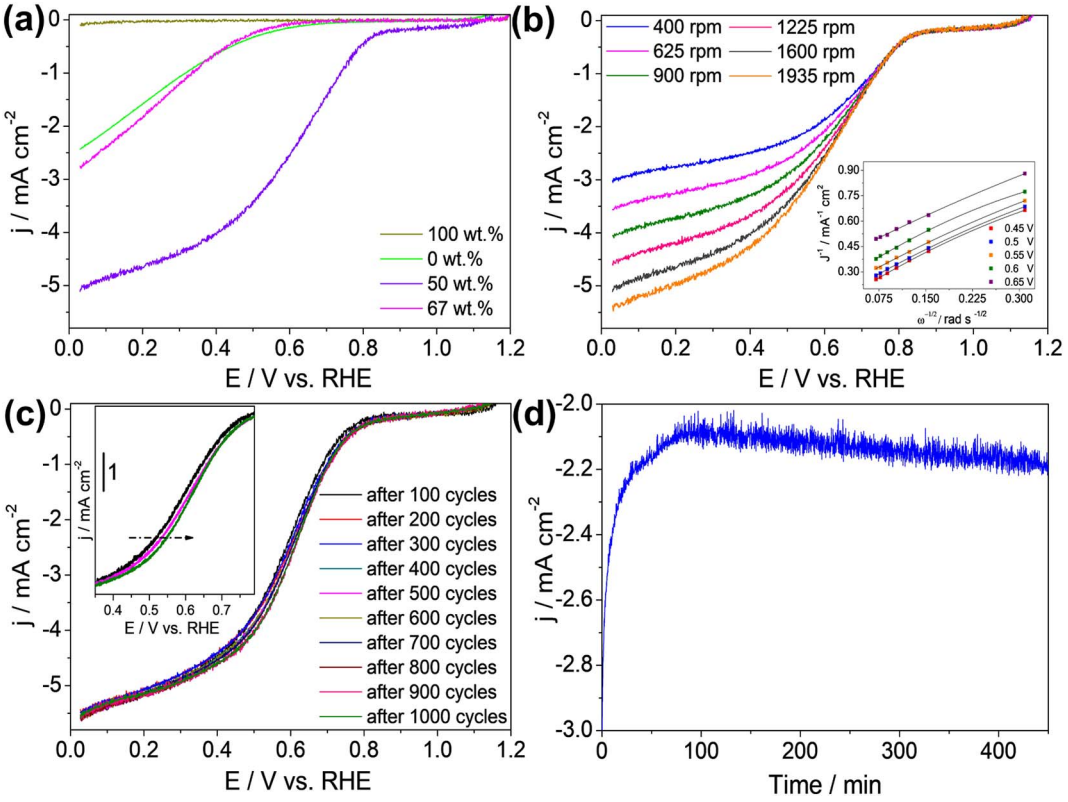

Fig. 3. (a) LSV data for the $FeCo_{14}Zn_{23}$/N/C composite mixed with different amounts of Vulcan XC-72, (b) LSV data for a 50:50 mixture of $FeCo_{14}Zn_{23}$/N/C and Vulcan XC-72 recorded at a different rotation speeds with K–L plots in the inset, (c) LSV data for the 50:50 mixture of $FeCo_{14}Zn_{23}$/N/C and Vulcan XC-72, recorded after every 100 CV cycles, (d) Chronoamperometry with the rotation speed of the electrode set at 1600 rpm. Experiments were carried out in O_2-saturated 0.1 M $HClO_4$ solution at 25 °C.

been proposed [16]. A possible tip-growth mechanism for nitrogen-doped carbon nanotubes catalyzed by iron NPs has also been described previously [17].

The surface of the $FeCo_{14}Zn_{23}$/N/C composite can be seen from the SEM micrograph in Fig. 2e, and the morphology is preserved after 1000 cycles of electrochemical testing, as shown in Fig. 2f.

LSV curves measured for different compositions of ink are illustrated in Fig. 3a. On its own, the $FeCo_{14}Zn_{23}$/N/C composite exhibited rather low catalytic activity. Vulcan itself does not possess any appreciable catalytic activity; its presence in the catalyst did not change the profile of the LSV curve. The highest catalytic activity was observed when a mixture containing equal portions of $FeCo_{14}Zn_{23}$/N/C and Vulcan was used. This weight composition (50:50) was chosen for the rest of the tests.

The ORR kinetics were investigated using Koutecky–Levich (K–L) plots [18]. The curves measured for the 50:50 electrode material are presented in Fig. 3b. For K–L plots from 0.45 to 0.65 V, the calculated electron transfer number, *n*, was found to vary from 3.6 to 4.3, suggesting a 4-electron pathway for the ORR. The linearity and near parallelism of the fitting lines are indicative of first-order reaction kinetics. The same electron transfer number, confirming the 4e-ORR reaction path, was observed for Fe/N/C, Pt/C [9] and Co/N/C [19] catalysts.

The exchange current density calculated from the intercept of a linear Tafel plot was $2.4{\cdot}10^{-8}$ A·cm^{-2}, close to the corresponding values for Pt/C and HDCMs. For instance, for the Pt/C catalyst TEC 10E50E with 46 wt% Pt (Tanaka Kikinzoku Kogyo Corp.) the value of $3.9{\cdot}10^{-8}$ A·cm^{-2} was reported [20]. For Fe-doped composites prepared by a multistep pyrolysis, the exchange current densities were estimated to be $1.1 \cdot 10^{-10}$–$4.6 \cdot 10^{-11}$ A·cm^{-2}. Wu et al. [21] reported exchange current densities of $4{\cdot}10^{-8}$ and $5 \cdot 10^{-10}$ A·cm^{-2} for Fe/N/C and Co/N/C catalysts, respectively. Depending on Fe content, Fe/N/C catalysts have been shown to exhibit higher exchange current densities ranging from $2.2{\cdot}10^{-6}$ to $4.1{\cdot}10^{-7}$ A·cm^{-2} [22].

The stability of the catalyst was tested during a long period of cycling. LSV curves recorded after every 100th CV cycle are presented in Fig. 3c. During cycling, the E_{onset} value shifted from 0.762 to 0.772 V, and the half-wave potential ($E_{1/2}$) value shifted from 0.605 V after 100 cycles to 0.617 V after 1000 cycles. This performance suggests that the catalyst's properties improved during cycling over the period studied.

The long-term stability of the $FeCo_{14}Zn_{23}$/N/C composite was tested by chronoamperometry (Fig. 3d) at $E = 0.6$ V (vs. RHE). The catalyst is durable over time and its performance even improved after 100 min of testing.

It is well known that addition of carbon to a catalyst during synthesis can control its morphology, enhance its activity, and improve its performance durability [23]. The mixtures containing both Vulcan and the composite appear to be more hydrophilic than the composite alone. As a result, the spread of the catalytic inks was improved when the mixture was used, so the working surface area of the catalytic layer was increased. This suggests that the addition of Vulcan carbon to the catalyst caused it to disaggregate, resulting in better dispersion in the ink. As a result, a higher proportion of catalyst particles become available to participate in the catalytic reaction.

In conclusion, we successfully developed a step-by-step approach to produce a precious-metal-free bamboo-like electrocatalyst for the ORR. The catalyst demonstrated high catalytic activity and stability in an acidic medium. The addition of an equal weight of Vulcan XC-72 to the catalytic ink improved its properties because spreading was facilitated, allowing a larger area of the catalyst to take part in the ORR.

Acknowledgments

This work was supported by the project of the Russian Science Foundation (grant no. 17-73-10386). We are grateful to Mary Bugaeva (SFedU) for graphical abstract design.

References

[1] S. Chu, A. Majumdar, Opportunities and challenges for a sustainable energy future, Nature 488 (2012) 294–303.

[2] M. Shao, Q. Chang, J.-P. Dodelet, R. Chenitz, Recent advances in electrocatalysts for oxygen reduction reaction, Chem. Rev. 116 (2016) 3594–3657.

[3] V.E. Guterman, T.A. Lastovina, S.V. Belenov, N.Y. Tabachkova, V.G. Vlasenko, I.I. Khodos, E.N. Balakshina, PtM/C (M = Ni, Cu, or Ag) electrocatalysts: effects of alloying components on morphology and electrochemically active surface areas, J. Solid State Electrochem. 18 (2014) 1307–1317.

[4] T. Lastovina, J. Pimonova, A. Budnyk, Platinum-free catalysts for low temperature fuel cells, J. Phys. Conf. Ser. 829 (2017) 012007.

[5] Q. Niu, J. Guo, B. Chen, J. Nie, X. Guo, G. Ma, Bimetal-organic frameworks/polymer core-shell nanofibers derived heteroatom-doped carbon materials as electrocatalysts for oxygen reduction reaction, Carbon 114 (2017) 250–260.

[6] Z. Li, M. Shao, L. Zhou, Q. Yang, C. Zhang, M. Wei, D.G. Evans, X. Duan, Carbon-based electrocatalyst derived from bimetallic metal-organic framework arrays for high performance oxygen reduction, Nano Energy 25 (2016) 100–109.

[7] M.H. Yap, K.L. Fow, G.Z. Chen, Synthesis and applications of MOF-derived porous nanostructures, Green Energy Environ. 2 (2017) 218–245.

[8] H. Zhang, H. Osgood, X. Xie, Y. Shao, G. Wu, Engineering nanostructures of PGM-free oxygen-reduction catalysts using metal-organic frameworks, Nano Energy 31 (2017) 331–350.

[9] Y. Wu, S. Zhao, K. Zhao, T. Tu, J. Zheng, J. Chen, H. Zhou, D. Chen, S. Li, Porous Fe-Nx/C hybrid derived from bi-metal organic frameworks as high efficient electrocatalyst for oxygen reduction reaction, J. Power Sources 311 (2016) 137–143.

[10] T. Palaniselvam, B.P. Biswal, R. Banerjee, S. Kurungot, Zeolitic imidazolate framework (ZIF)-derived, hollow-core, nitrogen-doped carbon nanostructures for oxygen reduction reactions in PEFCs, Chem. Eur. J. 19 (2013) 9335–9342.

[11] C. He, T. Zhang, F. Sun, C. Li, Y. Lin, Fe/N co-doped mesoporous carbon nanomaterial as an efficient electrocatalyst for oxygen reduction reaction, Electrochim. Acta 231 (2017) 549–556.

[12] J. Xi, Y. Xia, Y. Xu, J. Xiao, S. Wang, (Fe,Co)@nitrogen-doped graphitic carbon nanocubes derived from polydopamine-encapsulated metal–organic frameworks as a highly stable and selective non-precious oxygen reduction electrocatalyst, Chem. Commun. 51 (2015) 10479–10482.

[13] Y. Wang, X. Chen, Q. Lin, A. Kong, Q.-G. Zhai, S. Xie, P. Feng, Nanoporous carbon derived from a functionalized metal–organic framework as a highly efficient oxygen reduction electrocatalyst, Nano 9 (2017) 862–868.

[14] M. Rauf, Y.-D. Zhao, Y.-C. Wang, Y.-P. Zheng, C. Chen, X.-D. Yang, Z.-Y. Zhou, S.-G. Sun, Insight into the different ORR catalytic activity of Fe/N/C between acidic and alkaline media: protonation of pyridinic nitrogen, Electrochem. Commun. 73 (2016) 71–74.

[15] K.S. Park, Z. Ni, A.P. Côté, J.Y. Choi, R. Huang, F.J. Uribe-Romo, H.K. Chae, M. O'Keeffe, O.M. Yaghi, Exceptional chemical and thermal stability of zeolitic imidazolate frameworks, Proc. Natl. Acad. Sci. 103 (2006) 10186–10191.

[16] E.F. Kukovitsky, S.G. L'vov, N.A. Sainov, VLS-growth of carbon nanotubes from the vapor, Chem. Phys. Lett. 317 (2000) 65–70.

[17] X. Wang, W. Hu, Y. Liu, C. Long, Y. Xu, S. Zhou, D. Zhu, L. Dai, Bamboo-like carbon nanotubes produced by pyrolysis of iron(II) phthalocyanine, Carbon 39 (2001) 1533–1536.

[18] F.J. Vidal-Iglesias, J. Solla-Gullón, V. Montiel, A. Aldaz, Errors in the use of the Koutecky–Levich plots, Electrochem. Commun. 15 (2012) 42–45.

[19] J. Yang, L. Li, H. Yu, H. Geng, C. Li, X. Dong, Co/N-C nanotubes with increased coupling sites by space-confined pyrolysis for high electrocatalytic activity, Green Energy Environ. 2 (2017) 23–29.

[20] A. Muthukrishnan, Y. Nabae, T. Hayakawa, T. Okajima, T. Ohsaka, Fe-containing polyimide-based high-performance ORR catalysts in acidic medium: a kinetic approach to study the durability of catalysts, Cat. Sci. Technol. 5 (2015) 475–483.

[21] G. Wu, K.L. More, C.M. Johnston, P. Zelenay, High-performance electrocatalysts for oxygen reduction derived from polyaniline, iron, and cobalt, Science 332 (2011) 443–447.

[22] L. Zhang, K. Lee, C.W.B. Bezerra, J. Zhang, J. Zhang, Fe loading of a carbon-supported Fe–N electrocatalyst and its effect on the oxygen reduction reaction, Electrochim. Acta 54 (2009) 6631–6636.

[23] G. Wu, A. Santandreu, W. Kellogg, S. Gupta, O. Ogoke, H. Zhang, H.-L. Wang, L. Dai, Carbon nanocomposite catalysts for oxygen reduction and evolution reactions: from nitrogen doping to transition-metal addition, Nano Energy 29 (2016) 83–110.